Spectral Observations of Optical Emissions Associated with Terrestrial Gamma-Ray Flashes

Matthias Heumesser[1], Olivier Chanrion[1], Torsten Neubert[1], Hugh Christian[2], Christoph Koehn[1], Krystallia Dimitriadou[3], Francisco J Gordillo-Vazquez[4], Alejandro Luque[4], Francisco J. Pérez-Invernón[5], Richard Blakeslee[6], Andrew Mezentsev[7], Nikolai Østgaard[7], and Víctor Reglero[8]

[1]National Space Institute, Technical University of Denmark (DTU Spac), Denmark
[2]Earth System Science Center, University of Alabama in Huntsville, Alabama, USA
[3]Natinal Space Institute, Technical University of Denmark (DTU Space), Denmark
[4]Instituto de Astrofisica de Andalucıa (IAA
[5]Institut für Physik der Atmosphäre, Deutsches Zentrum für Luft- und Raumfahrt, Wessling, Germany
[6]NASA Marshall Space Flight Center, Huntsville, Alabama, USA
[7]Birkeland Centre for Space Science, University of Bergen, Bergen, Norway
[8]Image Processing Laboratory, University of Valencia, Valencia, Spain

November 22, 2022

Abstract

The Atmosphere-Space Interactions Monitor measures Terrestrial Gamma-Ray Flashes (TGFs) simultaneously with optical emissions from associated lightning activity. We analyzed optical measurements at 180-230 nm, 337 nm and 777.4 nm related to 69 TGFs observed between June 2018 and October 2019. All TGFs are associated with optical emissions with 90% at the onset of a large optical pulse, suggesting that they are connected with the initiation of current surges. A simple model of photon delay induced by cloud scattering suggests that the sources of the optical pulses are from 0.7 ms before to 4.4 ms after the TGFs, with a median of -10±80 µs, and 1-5 km below the cloud top. The pulses have rise times comparable to lightning without identified TGFs, while the FWHM is twice as long. Pulse amplitudes at 337 nm are 3 times larger than at 777.4 nm. The results support the leader-streamer mechanism for TGF generation.

Spectral Observations of Optical Emissions Associated with Terrestrial Gamma-Ray Flashes

Matthias Heumesser[1], Olivier Chanrion[1], Torsten Neubert[1], Hugh Christian[2], Christoph Köhn[1], Krystallia Dimitriadou[1], Francisco J. Gordillo-Vazquez[3], Alejandro Luque[3], Francisco Javier Pérez-Invernón[3,4], Richard J. Blakeslee[5], Andrey Mezentsev[6], Nikolai Østgaard[6] and Victor Reglero[7].

[1]National Space Institute, Technical University of Denmark (DTU Space), Denmark
[2]Earth System Science Center, University of Alabama in Huntsville, Alabama, USA
[3]Instituto de Astrofísica de Andalucía (IAA, CSIC), Granada, Spain
[4]Institut für Physik der Atmosphäre, Deutsches Zentrum für Luft- und Raumfahrt, Wessling, Germany
[5]NASA Marshall Space Flight Center, Huntsville, Alabama, USA
[6]Birkeland Centre for Space Science, University of Bergen, Bergen, Norway
[7]Image Processing Laboratory, University of Valencia, Valencia, Spain

Key Points:

- We present the first statistical analysis of emissions at 180-230 nm, 337 nm and 777 nm coincident with TGFs as measured by a single platform
- 90% of TGFs occur at the onset of large-amplitude optical pulses and thus support the streamer-leader model for TGF generation
- The sources of the emissions are estimated to be 1-5 km below the cloud tops

Index Terms:

ASIM, ISS, Optical Radiation, TGF, Streamer, Leader

Corresponding author: Matthias Heumesser, `heumat@space.dtu.dk`

Abstract

The Atmosphere-Space Interactions Monitor measures Terrestrial Gamma-Ray Flashes (TGFs) simultaneously with optical emissions from associated lightning activity. We analyzed optical measurements at 180-230 nm, 337 nm and 777.4 nm related to 69 TGFs observed between June 2018 and October 2019. All TGFs are associated with optical emissions with 90% at the onset of a large optical pulse, suggesting that they are connected with the initiation of current surges. A simple model of photon delay induced by cloud scattering suggests that the sources of the optical pulses are from 0.7 ms before to 4.4 ms after the TGFs, with a median of -10±80 µs, and 1-5 km below the cloud top. The pulses have rise times comparable to lightning without identified TGFs, while the FWHM is twice as long. Pulse amplitudes at 337 nm are ∼3 times larger than at 777.4 nm. The results support the leader-streamer mechanism for TGF generation.

Plain Language Summary

Terrestrial Gamma-Ray Flashes (TGFs) are short bursts of high-energy radiation produced in thunderstorms, first observed from astrophysical spacecraft during the 1990s. This study characterizes optical emissions from lightning associated with these flashes in multiple wavelengths to help finding their production mechanism. The data are collected by space based instruments aboard the International Space Station as it passes over the major thunderstorm regions of the Earth. We find that TGFs are associated with propagation of intra-cloud lightning in the upper cloud levels. With the help of a model of light propagation through a cloud, we estimate the source of the respective optical emissions to be 1-5 km below the cloud tops. By investigating TGFs and their connection to lightning, we can understand the energy- and timescales of lightning better, eventually leading to a better understanding of cloud physics and thunderstorms in general.

1 Introduction

Terrestrial Gamma-Ray Flashes (TGFs) are bursts of X- and gamma-rays from thunderstorms (Fishman et al., 1994). They are bremsstrahlung from relativistic runaway electrons, powered by the electric fields within the thunderstorm clouds (Wilson, 1925; Gurevich et al., 1992). The bursts last between ten and a few hundred microseconds (Marisaldi et al., 2014; Østgaard, Neubert, et al., 2019) with detected photon energies up to 40 MeV (Marisaldi et al., 2019). To explain the observed photon fluxes, one model considers amplification of the electron flux in impulsive, 10-100 meter-scale, intense electric fields at the tip of lightning leaders (Moss et al., 2006; Celestin & Pasko, 2011; Xu et al., 2012; da Silva & Pasko, 2013; Chanrion et al., 2014; Köhn et al., 2017). In this scenario, TGFs would always be associated with optical radiation from leaders. In another model, the electron flux is created by the kilometer-scale electric fields within the clouds via backscattered X-rays and inversely propagating positrons, created by pair production to seed additional avalanches. This feedback mechanism suggests the TGF production to be associated with modest levels of optical emissions if it is acting alone (Dwyer, 2008). Leader fields can help reaching the field threshold for the feedback mechanism.

Recent observations have shown that TGFs occur at the onset of optical emissions, which point to the importance of the lightning leader process (Neubert et al., 2020; Østgaard, Neubert, et al., 2019). The measurements were by the Atmosphere-Space Interactions Monitor (ASIM) on the International Space Station (ISS) that carries sensors in selected bands in the range from the infra-red to gamma-ray energies. With sensors on a common platform, ambiguities in the relative timing of the sensor data are reduced, a problem that has followed past studies attempting to correlate data from different satellites or on the ground (Østgaard et al., 2013; Gjesteland et al., 2017; Alnussirat et al., 2019).

In the study presented here, we analyze the UV and optical emissions detected by ASIM in connection with TGFs observed in the period from June 2018 to October 2019. We characterize the emissions relative to the TGF onset time, relate them to lightning propagation scenarios, and estimate their depth within the clouds. Section 2 gives an overview of the ASIM instruments, the data and the analysis methods; Section 3 presents the results and Section 4 a discussion.

2 Measurements and Analysis

ASIM on the ISS is designed to observe lightning, TGFs and Transient Luminous Events (TLEs) (Neubert et al., 2019). The instruments include the Modular Multi-spectral Imaging Array (MMIA) and the Modular X- and Gamma-ray Sensor (MXGS), both pointing towards nadir. The MXGS has a high-energy detector ($\sim$0.3 to >30 MeV) that measures day and night with a time resolution of 28.7 ns and a low-energy detector ($\sim$50-400 keV) that measures with a time resolution of 1 µs, but only during the night because of optical photon contamination (Østgaard, Balling, et al., 2019). The MMIA includes three photometers and two cameras with the same field of view. The photometers sample at 100 kHz at 180-230 nm (UV), which includes part of the N_2 Lyman-Birge-Hopfield lines, at 337/4 nm (blue) (center of band/bandwidth) that includes the strongest line of $N_2$2P, and at 777.4/5 nm (red), an OI line considered one of the strongest emission lines of the lightning spectrum. The cameras capture 12 frames per second at 337/4 nm and 777.4/3 nm with $\sim$400x400 m ground resolution at nadir (Chanrion et al., 2019). MMIA is only operational during night to prevent damage by sunlight. The instrument computers include flash trigger logic that saves all sensor data if one sensor detects a flash.

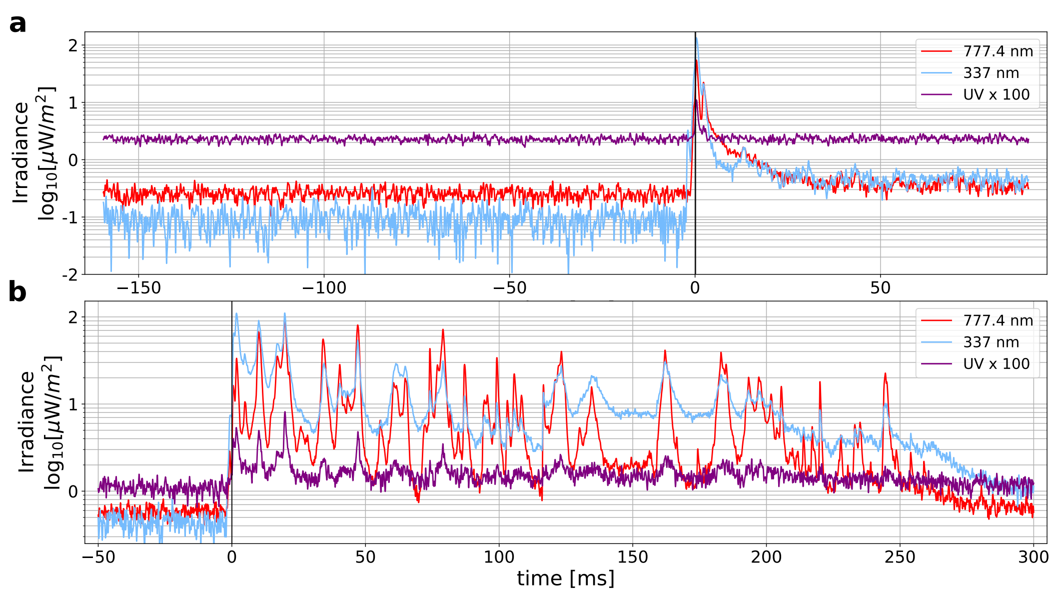

Figure 1. Typical optical signals observed in relation to TGFs. Time is relative to the detection of the first TGF photon on 26 May 2019, 02:29:34.993 **(a)** and 28 July 2018, 17:03:15.848 **(b)**.

In the period extending from the end of the commissioning phase on 2 June 2018 to 26 October 2019, ASIM observed 69 TGFs during the night inside the field of view (FOV) of the MMIA, all associated with optical emissions. The selected events where not associated with activity outside the MMIA FOV but inside the larger FOV of the Lightning Imaging Sensor on the ISS (ISS-LIS), rectangular with a diagonal of 1000 km (Blakeslee, 2019; Blakeslee et al., 2020), or the GLD360 network in a box of $\pm 6°$ latitude and longitude; both within a 200 ms window centered at the TGF time. The likelyhood that the TGF events are associated with lightning activity not observed by the MMIA is then reduced. During the first ten months of nominal operation, the relative timing uncertainty between the MXGS and MMIA was up to ± 80 µs, improving to ± 5 µs after a software update in April 2019 (Østgaard, Neubert, et al., 2019). The absolute time accuracy is better than 25 ms, but can often be improved to ~ 1 ms by correlation with ground-based lightning detection data from, for instance, GLD360 and data from ISS-LIS. Such corrective improvement was possible for nearly 90% of the cases considered here.

Two examples of the optical signals measured by the photometers are shown in Figure 1. In both cases, the TGFs are preceded by lower level pre-activity and are followed by high amplitude emissions. In the less common case (Figure 1a), the TGFs are followed by few pulses, but more often they are followed by a longer sequence of pulses (Figure 1b). In the analysis, we focus on a ± 20 ms time interval around the TGFs that includes the lower level activity prior to a TGF and the pulses that follow immediately after, but excludes continued, longer-duration activity after a TGF.

The optical signals are affected by photon scattering and absorption by cloud particles, which determine the shape of the recorded light curve (Thomason & Krider, 1982; Koshak et al., 1994; Light et al., 2001). A convenient way to estimate scattering properties is offered by Soler et al. (2020) and Luque et al. (2020). They present a model of an instantaneous, point-like source inside a planar, homogeneous cloud, where the normalized function describing the pulse shape observed above a cloud is:

$$f(t, t_0, \tau, \nu) = \sqrt{\frac{\tau}{\pi (t - t_0)^3}} \;\; \exp\left(2\sqrt{\nu\tau} - \frac{\tau}{t - t_0} - \nu(t - t_0)\right); \quad t > t_0 \qquad (1)$$

where t is time, t_0 is the time when the source releases photons, τ is the characteristic diffusion time and ν is the absorption rate. For those TGF events that are associated with a simple optical pulse, we subtract the average background noise level, i.e. the radiance before the pre-activity in the interval [-150, -20] in Figure 1a before scaling and fitting the function to the pulse. The fitting procedure is illustrated in Figure 2 for the cases of modest pre-pulse activity (a) and high pre-pulse activity (b). Higher pre-pulse activity increases the uncertainties of the three fitting parameters, as discussed in a later section. We use the fitted function to define the times $\mathrm{t_x}$ where the pulses reach x% of their signal maximum and derive parameters such as the rise time, t_{90} - t_{10}, or the duration of full width at half maximum (FWHM), t_{50t} - t_{50}; $\mathrm{t_{xt}}$ denotes the times in the decaying tail of the pulse.

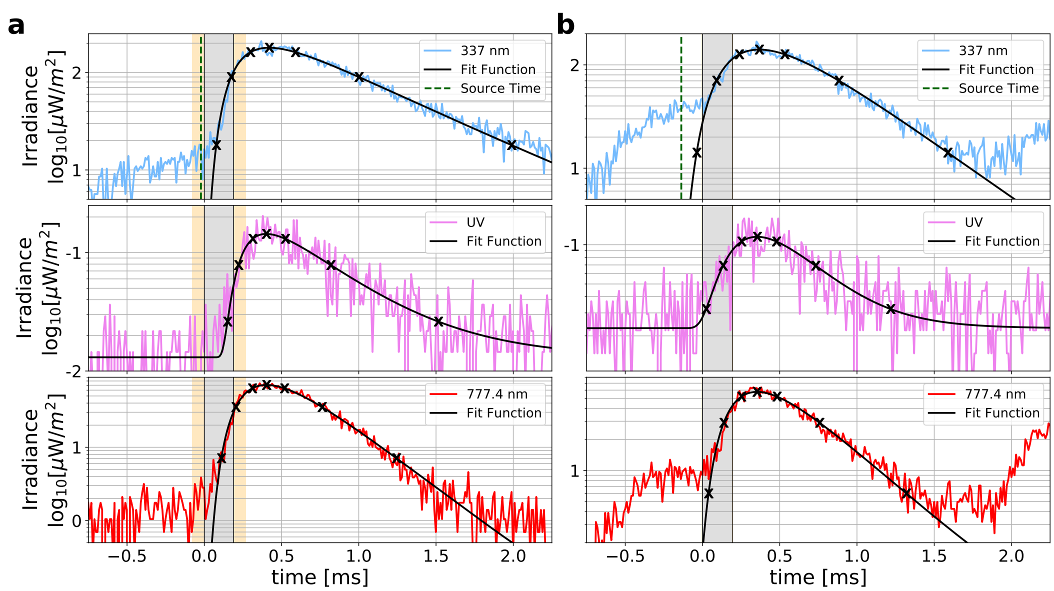

Figure 2. The functional fit to the photometer signals. **a)** Modest pre-pulse activity, **b)** high pre-pulse activity. A time of 0 ms is the start time of the TGF, the grey shaded region marks the duration of the TGF and the orange shaded region the respective time uncertainty of the measurement (±80 and ±5 µs). The source time t_0 is indicated with a green, dashed line in the 337 nm band, crosses mark f_{10}, f_{50}, f_{90}, f_{max}, f_{90t}, f_{50t}, f_{10t} and thus the corresponding t_x and t_{xt}.

To estimate the physical nature of the cloud scattering that can be derived from the function, we chose the blue band and fit only the first half of the pulse to obtain new values for t_0 and τ. This wavelength is the least affected by absorption and the first half of the pulses is from photons that have undergone the least scattering in the cloud. They are therefore the least depndent on the model assumption of an horizontally infinite cloud.

A simulation model of photon scattering in arbitrary cloud geometries is described in Luque et al. (2020).

With τ, we can estimate the depth of the optical sources inside the clouds. Therefore, we need to make assumptions regarding size distribution and density of the cloud hydrometeors. These assumptions do not impact on the fitting of τ and get important solely in estimating the depths. The depth inside the cloud depends on τ and the diffusion coefficient, D, as $L = \sqrt{4D\tau}$. The diffusion coefficient is $D = \Lambda c/3(1 - g\omega_0)$ where Λ is the mean free path of photons, c is the speed of light, g is a wavelength dependent asymmetry factor and ω_0 is the single scattering albedo. At 337 nm, $g \sim 0.88$ and $\omega_0 \sim 1$. The mean free path depends on the size, r_c, and density, n_c, distributions of cloud particles as $\Lambda = 1/(2\pi r_c^2 n_c)$ (Thomason & Krider, 1982; Koshak et al., 1994; Light et al., 2001; Soler et al., 2020). Thus, we estimate L based on τ and the assumptions for n_c, r_c, g and ω_0.

3 Results

Of the 69 TGFs selected for analysis, 62 were followed by a strong optical pulse at 337 and 777.4 nm, which could be fitted with the function in Equation (1) in 52 cases. In the UV, 14 observations have pulses that could be fitted. We do not include three simultaneous Elve detections, the luminous emissions in the ionosphere due to excitation by strong electromagnetic pulses from lightning, because of their different origin above the clouds (Neubert et al., 2020).

The results of the fits are summarized in Figure 3. The median source time t_0 is -10±80 µs relative to the first photon of the TGFs with outliers up to several ms (t_0 is only determined for the blue signal). The rise times are ∼260-370 µs and the FWHM is around 1 ms. The FWHM is somewhat larger for 337 nm than for 777.4 nm, consistent with more scattering of the blue photons and higher absorption of the red photons. Compared to statistics of lighting flashes without identified TGFs (Offroy et al., 2015; Christian & Goodman, 1987), the pulses presented here exhibit slightly longer rise times, +50-100 µs, and doubled FWHMs, ∼1-1.5 ms. The time parameters of UV emissions are more similar to the red than to the blue, but suffer generally most from atmospheric absorption (Luque et al., 2020; Molina & Molina, 1986). Neither rise time nor FWHM are affected by the instrumental timing uncertainty. More values are given in the supplement.

The majority of the source times is within the instrumental and model uncertainties of the TGF start. We conclude, then, that the majority of optical pulses are emitted at the onset of TGFs, consistent with previous case studies (Neubert et al., 2020; Østgaard, Neubert, et al., 2019; Alnussirat et al., 2019), with some cases delayed up to ∼4 ms. The uncertainties are discussed further in the next section. The optical source duration is modeled by a function that describes an instantaneous source, suggesting that the pulse duration may be caused by cloud scattering, just as TGF pulses are broadened by Compton scattering of the photons (Celestin & Pasko, 2012). Both sources, optical and gamma ray, are then likely of comparable duration.

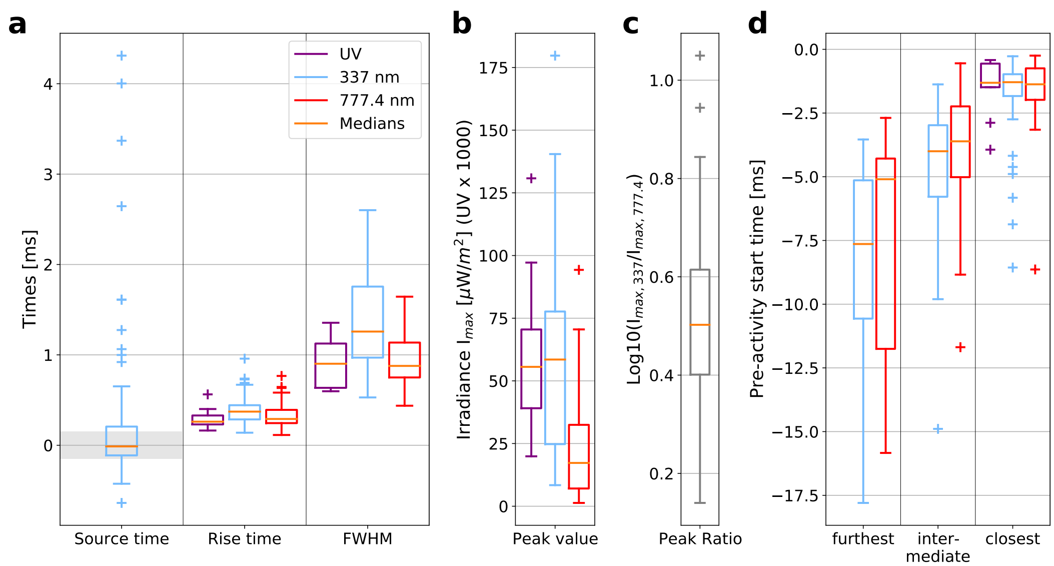

Figure 3. Characteristics of the optical peak following a TGF. The boxes represent the interquartile range of the values from the 25th to 75th percentile and the horizontal lines within are the median values. The whiskers extend to 1.5 times the interquartile range or to the maximum and minimum values if they are lower, outliers are shown as '+'. **a)** The temporal characteristics for each photometer band. From left to right they are the source time (t_0) relative to the arrival of the first TGF photon, the rise time and the FWHM. The grey shaded area in the interval [-0.15, 0.15] ms indicates the uncertainty as discussed later. **b)** Irradiance of the optical pulses in the three bands. The irradiance in the UV band is multiplied by 1000 to show it on the same scale as the other bands. **c)** Ratio of the peak values of 337 nm and 777 nm. **d)** start of the pre-activity pulses relative to start of the main pulse.

The peak irradiance in the blue is generally ∼3 times stronger than in the red (Figures 3b,c), while 777.4 nm emissions dominate regular lightning pulses, i.e. ratios ≤1 (e.g.

Adachi et al., 2016). For the cases with UV pulses, the amplitudes of the blue and the UV correlate with a magnitude difference of 10^3.

Close to 90% of the TGF observations had corresponding ISS-LIS or GLD360 detections, matching in location inside the FOV and allowing us to correct the absolute timing. We find GLD and LIS detections, when available, to be associated with the main optical pulse, not the TGF itself. This has implications for studies that correlate TGF events with ground observations of lightning.

During the pre-activity, the red and blue photometer signals increased when approaching the onset of the main optical pulse, with 1-3 smaller pulses in the signal amplitude. The majority of observations had two pulses while a third had three pulses. In the UV band, 9 observations had one preceding pulse, more than one was not observed. The statistics of pre-activity start times in Figure 3d is sorted by the temporal proximity of the pulses to the main optical pulse and shows the intervals between the pulses shorten when approaching the main peak. Optical emissions more than 20 ms prior to the TGF from the same location were observed in 2 of the 52 cases. In both of them, the detections were of low intensity and dominantly blue, consistent with the the rest of the pre-activity measurements. Consequently, TGFs occur in the initial phase of a flash without extensive optical activity before them. Intensities and durations of the pre-activity pulses can be found in the supplement.

The depth in the clouds of the optical sources at TGF onset were estimated from the fit of the first half of the blue photometer signal, as described earlier. We assume a cloud top composition of water ice droplets with typical values $r_c = 15$, 20 µm and $n_c = 2.5 \cdot 10^8$ m^{-3} (Dye et al., 2007; Ursi et al., 2019) while also accounting for the direction from the source to the detector relative to zenith. The altitude is estimated by assuming the cloud tops are at the tropopause (Splitt et al., 2010; Ursi et al., 2019) and that the tropopause altitude follows Equation (2) of Offroy et al. (2015).

The result is shown in Figure 4. The optical sources that can be approximated by the fit function (75% of the events) are in the top of the cloud and at a few km depth, consistent with Stanley et al. (2006); Cummer et al. (2015). The depth and altitude depend on the parameters that enter the assumptions on the cloud particles, where less dense clouds, $r_c = 15$ µm, lead to greater depths. For $n_c = 10^8$ m^{-3}, the altitudes are 1-2 km lower.

We conclude this section by noting a simple method to estimate the parameter τ, which is the only pulse parameter entering the altitude estimation. We find it can be approximated from the FWHM as $\tau = k \cdot FWHM + d$ with $k = 0.853 \pm 0.29$ and $d = -0.001 \pm 0.429$, see also Figure S4 in the supplement.

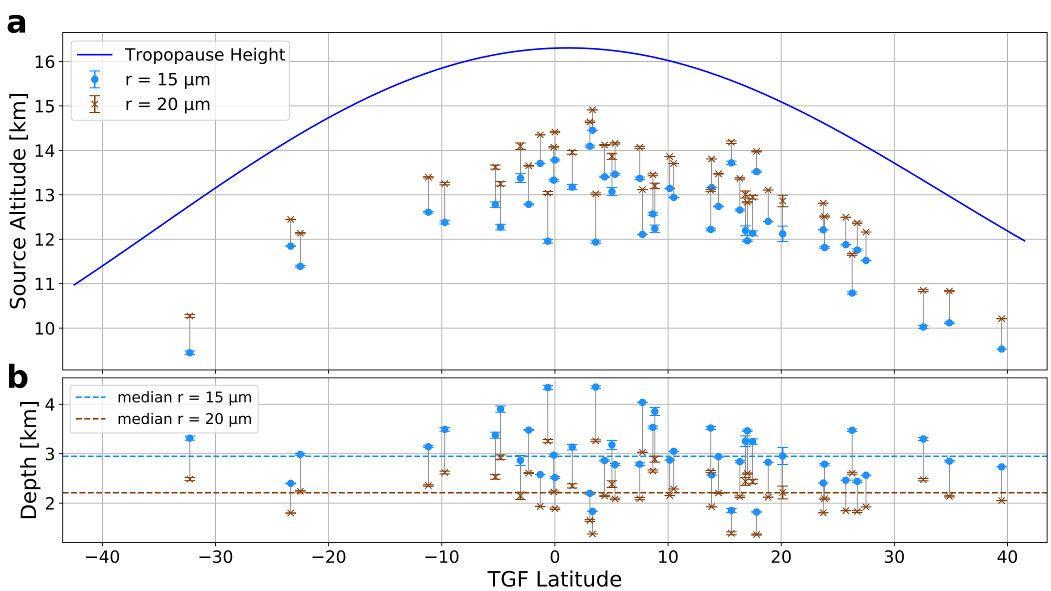

Figure 4. Estimated source altitudes **(a)** and depths inside clouds **(b)** of the optical pulses associated with TGFs for $n_c = 2.5 \cdot 10^8$ m^{-3}.

4 Discussion and Interpretation

Upward negative intra-cloud leaders in the upper cloud regions are thought to propagate from the central negative charge region towards the upper positive charge region while producing 1-3 bursts of initial breakdown pulses (IBPs) with 1-5 ms between the bursts. IBPs are signatures in signals measured by electric field sensors (Marshall et al., 2013). Video recordings from the ground show luminosity increases in the visible spectrum at the time of large IBPs (Stolzenburg et al., 2016). The observation of 1-3 pre-activity pulses with increasing intensity observed by ASIM agrees then well with upward propagating leaders that produce luminous IBP bursts (cf. supplementary Figure S2). Shorter intervals of the pulses (Figure 3d) further suggest an upward acceleration of the leaders as discussed in Cummer et al. (2015).

The characteristics of the main optical pulses associated with the TGFs appear consistent with the so-called energetic in-cloud pulses (EIPs) observed by ground networks in LF signals (30-300 kHz). EIPs are typically detected within a few ms after the initiation of upward negative leaders in the upper regions of the clouds (Lyu et al., 2015, 2016), as also seen in Figure 4. Whereas Lyu et al. (2018) find that at least some TGFs are associated with large currents, we find that all TGFs have associated red pulses, indicating significant leader current flow (e.g. Bitzer et al., 2016). The red signal is atypically weaker than the blue and both bands show twice as long pulse durations (FWHM) compared to normal lightning pulses without identified TGFs (Offroy et al., 2015; Christian & Goodman, 1987; Adachi et al., 2016). The similarity of the main pulse and EIP characteristics suggests the pulses to be the optical equivalent of EIPs.

The optical scattering properties of the cloud, estimated from the fit function, must be taken with caution since lightning is spatially and temporally extended. However, as long as the source onset is short compared to the rise times of the optical pulses, i.e. less than ∼100 µs, we find the fit function to the first half of the pulse, from which we stimate t_0 and τ, to be relativelty insensitive to the assumption on the temporal variation of the source. Nevertheless, the source duration is likely much shorter than the measured pulse durations and likely in the range of TGF sources, which are typically a few 100 µs or less (Marisaldi et al., 2014; Østgaard, Neubert, et al., 2019). As in scattering of optical emissions, TGFs are broadened by Compton scattering (Celestin & Pasko, 2012), indicating that the sources are a few tens of µs in duration. The average duration of EIPs in LF waveforms is 55 µs (Lyu et al., 2015). Consequently, all infered source durations related to TGF detection (LF, optical, TGF photons) are down to ∼10 to few 100 µs.

To investigate the accuracy of t_0, we derived t_0 from the red signal (leader emissions) and compared it to the start times of UV signatures of two cases with simultaneous Elves (powered by electromagnetic pulses from impulsive leader currents). We find $t_{0,red}$ to be 59±8 and 22±7 µs before the onset of the Elve emissions in the UV, while $t_{0,blue}$ was 113±6 and 99±8 µs earlier. Since Elve emissions are unaffected by cloud scattering, they are an estimate of the onset time of the current pulses. Elves are expanding rings in the lower ionosphere extending several 100 km in horizontal radius. The detection of their onset is typically ∼20 µs delayed due to the geometry of the emissions relative to the sensors. Accounting for this delay, $t_{0,red}$ is ∼40 and ∼0 µs before the Elve. However, this example also shows how the pre-activity interferes with the fitting procedure on this precise level: The Elve case with a 777-UV delay of 22/∼0 µs has a pre-activity intensity of <5%, while the maximum pre-activity intensity was ∼30% in the case with the larger delay (∼60/40 µs). Therefore, we have to assume that pre-activity levels above ∼20% of the main pulse intensity introduce methodical uncertainties of up to ∼30-40 µs, valid also for the blue activity and the respective t_0 values. Additional uncertainty is possibly introduced by Elve emissions in the blue band. From the cases studied, we expect intensities less than those in the UV, ∼3-4 $\mu W/m^2$, which are of the order of, or smaller than, the pre-activity. The analysis of the two Elves indicates the mutual production of the red leader emissions and the Elves, while the blue emissions appear to start before this phase.

With the instrumental and methodical uncertainties, ±80 or ±5 µs as mentioned earlier and ∼30-40 µs respectively, the median source time of the optical pulses at -10 µs before the TGF onset (Figure 3a) is smaller than the accuracy of the source time identification and does not allow to address the sequence of the events. For outliers more than ∼150 µs before or after the TGF onset, the sequence seems to be clear, provided we have identified the correct pulse associations with the TGF.

The consistent occurrence of optical signals in the blue and red bands for all TGFs connects TGF production to streamer and leader processes. Optical detections after the main peak, observed for some events (Figure 1b), is likely continued leader activity and branching in the cloud (Cummer et al., 2015). In our understanding, dominating blue emissions in the main pulses (Figure 3b,c) indicate high levels of streamer activity. Combined with measurements of VHF (30-300 MHz) activity related to TGFs by others, proposed to be a signature of temporally and spatially estended source regions (Lyu et al., 2018), we suggest a scenario where the optical and TGF emissions are generated as the atmosphere of the region ahead of the leader tip breaks down in a flash of streamers, high-energy electrons and a leader current surge.

Acknowledgments

MH appreciates discussions with and feedback from Joe Dwyer. We thank VAISALA for the GLD360 lightning data. **Funding:** ASIM is a mission of the European Space Agency (ESA) and is funded by ESA and by national grants of Denmark, Norway and Spain. The ASIM Science Data Centre is supported by ESA PRODEX contracts C 4000115884 (DTU) and 4000123438 (Bergen). The science analysis is supported by: the European Research Council grant n. 320839, the Research Council of Norway contracts 223252/F50 (CoE/BCSS), the Ministerio Ciencia e Innovacion grant ESP 2017- 86263-C4, and project grant PID2019-109269RB. This project has received funding from the European Union's Horizon 2020 research and innovation programme under the Marie Skłodowska-Curie grant agreement 722337. **Competing interests**: The authors declare no competing interests. **Data and materials availability**: ASIM data and Vaisala GLD360 detections are available via asdc.space.dtu.dk. ISS-LIS data is available from (Blakeslee, 2019)

References

Adachi, T., Sato, M., Ushio, T., Yamazaki, A., Suzuki, M., Kikuchi, M., … Kusunoki, K. (2016, jul). Identifying the occurrence of lightning and transient luminous events by nadir spectrophotometric observation. *Journal of Atmospheric and Solar-Terrestrial Physics*, *145*, 85–97. Retrieved from http://dx.doi.org/10.1016/j.jastp.2016.04.010https://linkinghub.elsevier.com/retrieve/pii/S1364682616301109 doi: 10.1016/j.jastp.2016.04.010

Alnussirat, S. T., Christian, H. J., Fishman, G. J., Burchfield, J., & Cherry, M. L. (2019, oct). Simultaneous space-based observations of terrestrial gamma-ray flashes and lightning optical emissions: Investigation of the terrestrial gamma-ray flash production mechanisms. *Physical Review D*, *100*(8), 083018 1–7. Retrieved from https://doi.org/10.1103/PhysRevD.100.083018https://link.aps.org/doi/10.1103/PhysRevD.100.083018 doi: 10.1103/PhysRevD.100.083018

Bitzer, P. M., Burchfield, J. C., & Christian, H. J. (2016, mar). A Bayesian Approach to Assess the Performance of Lightning Detection Systems. *Journal of Atmospheric and Oceanic Technology*, *33*(3), 563–578. Retrieved from http://journals.ametsoc.org/doi/10.1175/JTECH-D-15-0032.1 doi: 10.1175/JTECH-D-15-0032.1

Blakeslee, R. J. (2019). *Non-Quality Controlled Lightning Imaging Sensor (LIS) on International Space Station (ISS) Science Data.* NASA Global Hydrology Resource Center DAAC, Huntsville, Alabama, U.S.A. Retrieved from http://https//ghrc.nsstc.nasa.gov/hydro/details/isslis_v1_nqc doi: http://dx.doi.org/10.5067/LIS/ISSLIS/DATA107

Blakeslee, R. J., Lang, T. J., Koshak, W. J., Buechler, D., Gatlin, P., Mach, D. M., … Christian, H. (2020, jul). Three years of the Lightning Imaging Sensor onboard the International Space Station: Expanded Global Coverage and Enhanced Applications. *Journal of Geophysical Research: Atmospheres*, 1–20. Retrieved from `https://onlinelibrary.wiley.com/doi/abs/10.1029/2020JD032918` doi: 10.1029/2020JD032918

Celestin, S., & Pasko, V. P. (2011, mar). Energy and fluxes of thermal runaway electrons produced by exponential growth of streamers during the stepping of lightning leaders and in transient luminous events. *Journal of Geophysical Research: Space Physics*, *116*(A03315), 1–14. Retrieved from `http://doi.wiley.com/10.1029/2010JA016260` doi: 10.1029/2010JA016260

Celestin, S., & Pasko, V. P. (2012, jan). Compton scattering effects on the duration of terrestrial gamma-ray flashes. *Geophysical Research Letters*, *39*(2). Retrieved from `http://doi.wiley.com/10.1029/2011GL050342` doi: 10.1029/2011GL050342

Chanrion, O., Bonaventura, Z., Çinar, D., Bourdon, A., & Neubert, T. (2014, may). Runaway electrons from a beam-bulk' model of streamer: application to TGFs. *Environmental Research Letters*, *9*(5), 055003. Retrieved from `https://iopscience.iop.org/article/10.1088/1748-9326/9/5/055003` doi: 10.1088/1748-9326/9/5/055003

Chanrion, O., Neubert, T., Lundgaard Rasmussen, I., Stoltze, C., Tcherniak, D., Jessen, N. C., … Lorenzen, M. (2019, jun). The Modular Multispectral Imaging Array (MMIA) of the ASIM Payload on the International Space Station. *Space Science Reviews*, *215*(4), 28. Retrieved from `http://dx.doi.org/10.1007/s11214-019-0593-yhttp://link.springer.com/10.1007/s11214-019-0593-y` doi: 10.1007/s11214-019-0593-y

Christian, H. J., & Goodman, S. J. (1987, dec). Optical Observations of Lightning from a High-Altitude Airplane. *Journal of Atmospheric and Oceanic Technology*, *4*(4), 701–711. Retrieved from `http://journals.ametsoc.org/doi/abs/10.1175/1520-0426%281987%29004%3C0701%3AOOOLFA%3E2.0.CO%3B2` doi: 10.1175/1520-0426(1987)004⟨0701:OOOLFA⟩2.0.CO;2

Cummer, S. A., Lyu, F., Briggs, M. S., Fitzpatrick, G., Roberts, O. J., & Dwyer, J. R. (2015). Lightning leader altitude progression in terrestrial gamma-ray flashes. *Geophysical Research Letters*, *42*(18), 7792–7798. doi: 10.1002/2015GL065228 da Silva, C. L., & Pasko, V. P. (2013, dec). Dynamics of streamer-to-leader transition at reduced air densities and its implications for propagation of lightning leaders and gigantic jets. *Journal of Geophysical Research: Atmospheres*, *118*(24), 13,561–13,590. Retrieved from `http://doi.wiley.com/10.1002/2013JD020618` doi: 10.1002/2013JD020618

Dwyer, J. R. (2008, may). Source mechanisms of terrestrial gamma-ray flashes. *Journal of Geophysical Research*, *113*(D10), D10103. Retrieved from `http://doi.wiley.com/10.1029/2007JD009248` doi: 10.1029/2007JD009248

Dye, J. E., Bateman, M. G., Christian, H. J., Defer, E., Grainger, C. A., Hall, W. D., ... Willis, P. T. (2007, jun). Electric fields, cloud microphysics, and reflectivity in anvils of Florida thunderstorms. *Journal of Geophysical Research*, *112*(D11), D11215. Retrieved from `http://doi.wiley.com/10.1029/2006JD007550` doi: 10.1029/2006JD007550

Fishman, G. J., Bhat, P. N., Mallozzi, R., Horack, J. M., Koshut, T., Kouveliotou, C., ... Goodman, S. J. (1994). Discovery of Intense Gamma-Ray Flashes of Atmospheric Origin. *Science*, *264*(5163), 1313–1316.

Gjesteland, T., Østgaard, N., Bitzer, P., & Christian, H. J. (2017, jul). On the timing between terrestrial gamma ray flashes, radio atmospherics, and optical lightning emission. *Journal of Geophysical Research: Space Physics*, *122*(7), 7734–7741. Retrieved from `http://doi.wiley.com/10.1002/2017JA024285` doi: 10.1002/2017JA024285

Gurevich, A., Milikh, G., & Roussel-Dupre, R. (1992, jun). Runaway electron mechanism of air breakdown and preconditioning during a thunderstorm. *Physics Letters A*, *165*(5-6), 463–468. Retrieved from `https://linkinghub.elsevier.com/retrieve/pii/037596019290348P` doi: 10.1016/0375-9601(92)90348-P

Köhn, C., Diniz, G., & Harakeh, M. N. (2017). Production mechanisms of leptons, photons, and hadrons and their possible feedback close to lightning leaders. *Journal of Geophysical Research*, *122*(2), 1365–1383. doi: 10.1002/2016JD025445

Koshak, W. J., Solakiewicz, R. J., Phanord, D. D., & Blakeslee, R. J. (1994). Diffusion model for lightning radiative transfer. *Journal of Geophysical Research*, *99*(D7), 14361–14371.

Light, T. E., Suszcynsky, D. M., Kirkland, M. W., & Jacobson, A. R. (2001, aug). Simulations of lightning optical waveforms as seen through clouds by satellites. *Journal of Geophysical Research: Atmospheres*, *106*(D15), 17103–17114. Retrieved from `http://doi.wiley.com/10.1029/2001JD900051` doi: 10.1029/2001JD900051

Luque, A., Gordillo-Vázquez, F. J., Li, D., Malagón-romero, A., Pérez-invernón, F. J., Schmalzried, A., … Østgaard, N. (2020). Modeling lightning observations from space-based platforms (CloudScat.jl 1.0). *Geoscientific Model Development Discussion*. doi: 10.5194/gmd-2020-161

Lyu, F., Cummer, S. A., Briggs, M., Marisaldi, M., Blakeslee, R. J., Bruning, E., … Stanbro, M. (2016, aug). Ground detection of terrestrial gamma ray flashes from distant radio signals. *Geophysical Research Letters*, *43*(16), 8728–8734. Retrieved from `http://doi.wiley.com/10.1002/2016GL070154` doi: 10.1002/2016GL070154

Lyu, F., Cummer, S. A., Krehbiel, P. R., Rison, W., Briggs, M. S., Cramer, E., … Stanbro, M. (2018, feb). Very High Frequency Radio Emissions Associated With the Production of Terrestrial Gamma-Ray Flashes. *Geophysical Research Letters*, *45*(4), 2097–2105. Retrieved from `http://doi.wiley.com/10.1002/2018GL077102` doi: 10.1002/2018GL077102

Lyu, F., Cummer, S. A., & McTague, L. (2015, aug). Insights into high peak current incloud lightning events during thunderstorms. *Geophysical Research Letters*, *42*(16), 6836–6843. Retrieved from `https://onlinelibrary.wiley.com/doi/abs/10.1002/2015GL065047` doi: 10.1002/2015GL065047

Marisaldi, M., Fuschino, F., Tavani, M., Dietrich, S., Price, C., Galli, M., … Vercellone, S. (2014, feb). Properties of terrestrial gamma ray flashes detected by AGILE MCAL below 30 MeV. *Journal of Geophysical Research: Space Physics*, *119*(2), 1337–1355. Retrieved from `http://doi.wiley.com/10.1002/2013JA019301` doi: 10.1002/2013JA019301

Marisaldi, M., Galli, M., Labanti, C., Østgaard, N., Sarria, D., Cummer, S. A., … Verrecchia, F. (2019, jul). On the HighEnergy Spectral Component and Fine Time Structure of Terrestrial Gamma Ray Flashes. *Journal of Geophysical Research: Atmospheres*, *124*(14), 7484–7497. Retrieved from `https://onlinelibrary.wiley.com/doi/abs/10.1029/2019JD030554` doi: 10.1029/2019JD030554

Marshall, T., Stolzenburg, M., Karunarathne, S., Cummer, S., Lu, G., Betz, H.-D., … Xiong, S. (2013, oct). Initial breakdown pulses in intracloud lightning flashes and their relation to terrestrial gamma ray flashes. *Journal of Geophysical Research: Atmospheres*, *118*(19), 10,907–10,925. Retrieved from `http://doi.wiley.com/10.1002/jgrd.50866` doi: 10.1002/jgrd.50866

Molina, L. T., & Molina, M. J. (1986). Absolute absorption cross sections of ozone in the 185- to 350-nm wavelength range. *Journal of Geophysical Research*, *91*(D13), 14501. Retrieved from `http://doi.wiley.com/10.1029/JD091iD13p14501` doi: 10.1029/JD091iD13p14501

Moss, G. D., Pasko, V. P., Liu, N., & Veronis, G. (2006). Monte Carlo model for analysis of thermal runaway electrons in streamer tips in transient luminous events and streamer zones of lightning leaders. *Journal of Geophysical Research*, *111*(A2), A02307. Retrieved from `http://doi.wiley.com/10.1029/2005JA011350` doi: 10.1029/2005JA011350

Neubert, T., Østgaard, N., Reglero, V., Blanc, E., Chanrion, O., Oxborrow, C. A., … Bhanderi, D. D. V. (2019, mar). The ASIM Mission on the International Space Station. *Space Science Reviews*, *215*(2), 26. Retrieved from `http://dx.doi.org/10.1007/s11214-019-0592-zhttp://link.springer.com/10.1007/s11214-019-0592-z` doi: 10.1007/s11214-019-0592-z

Neubert, T., Østgaard, N., Reglero, V., Chanrion, O., Heumesser, M., Dimitriadou, K., … Eyles, C. J. (2020, dec). A terrestrial gamma-ray flash and ionospheric ultraviolet emissions powered by lightning. *Science*, *367*(6474), 183–186. Retrieved from `https://science.sciencemag.org/content/367/6474/183https://www.sciencemag.org/lookup/doi/10.1126/science.aax3872` doi: 10.1126/science.aax3872

Offroy, M., Farges, T., Kuo, C. L., Chen, A. B. C., Hsu, R. R., Su, H. T., … Frey, H. U. (2015, aug). Temporal and radiometric statistics on lightning flashes observed from space with the ISUAL spectrophotometer. *Journal of Geophysical Research*, *120*(15), 7586–7598. Retrieved from `http://doi.wiley.com/10.1002/2015JD023263` doi: 10.1002/2015JD023263

Østgaard, N., Balling, J. E., Bjørnsen, T., Brauer, P., Budtz-Jørgensen, C., Bujwan, W., … Yang, S. (2019). The Modular X- and Gamma-Ray Sensor (MXGS) of the ASIM Payload on the International Space Station. *Space Science Re-*

views, *215* (2), 23. Retrieved from http://link.springer.com/10.1007/s11214-018-0573-7 doi: 10.1007/s11214-018-0573-7

Østgaard, N., Gjesteland, T., Carlson, B. E., Collier, A. B., Cummer, S. A., Lu, G., & Christian, H. J. (2013, may). Simultaneous observations of optical lightning and terrestrial gamma ray flash from space. *Geophysical Research Letters*, *40* (10), 2423–2426. Retrieved from http://doi.wiley.com/10.1002/grl.50466 doi: 10.1002/grl.50466

Østgaard, N., Neubert, T., Reglero, V., Ullaland, K., Yang, S., Genov, G., . . . Al-nussirat, S. (2019, dec). First 10 Months of TGF Observations by ASIM. *Journal of Geophysical Research: Atmospheres*, *124* , 2019JD031214. Retrieved from https://onlinelibrary.wiley.com/doi/abs/10.1029/2019JD031214 doi: 10.1029/2019JD031214

Soler, S., PérezInvernón, F. J., GordilloVázquez, F. J., Luque, A., Li, D., MalagónRomero, A., . . . Østgaard, N. (2020, jul). Blue optical observations of narrow bipolar events by ASIM suggest corona streamer activity in thunderstorms. *Journal of Geophysical Research: Atmospheres*. Retrieved from https://onlinelibrary.wiley.com/doi/abs/10.1029/2020JD032708 doi: 10.1029/2020JD032708

Splitt, M. E., Lazarus, S. M., Barnes, D., Dwyer, J. R., Rassoul, H. K., Smith, D. M., . . . Grefenstette, B. (2010, jun). Thunderstorm characteristics associated with RHESSI identified terrestrial gamma ray flashes. *Journal of Geophysical Research: Space Physics*, *115* (A6). Retrieved from http://doi.wiley.com/10.1029/2009JA014622 doi: 10.1029/2009JA014622

Stanley, M. A., Shao, X.-M., Smith, D. M., Lopez, L. I., Pongratz, M. B., Harlin, J. D., . . . Regan, A. (2006). A link between terrestrial gamma-ray flashes and intracloud lightning discharges. *Geophysical Research Letters*, *33* (6), L06803. Retrieved from http://doi.wiley.com/10.1029/2005GL025537 doi: 10.1029/2005GL025537

Stolzenburg, M., Marshall, T. C., Karunarathne, S., & Orville, R. E. (2016, sep). Luminosity with intracloud-type lightning initial breakdown pulses and terrestrial gamma-ray flash candidates. *Journal of Geophysical Research: Atmospheres*, *121* (18), 10,919–10,936. Retrieved from http://doi.wiley.com/10.1002/2016JD025202 doi: 10.1002/2016JD025202

Thomason, L. W., & Krider, E. P. (1982, sep). The Effects of Clouds on the Light Produced by Lightning. *Journal of the Atmospheric Sciences*, *39*(9), 2051–2065. Retrieved from `http://journals.ametsoc.org/doi/abs/10.1175/1520-0469%281982%29039%3C2051%3ATEOCOT%3E2.0.CO%3B2` doi: 10.1175/1520-0469(1982)039⟨2051:TEOCOT⟩2.0.CO;2

Ursi, A., Marisaldi, M., Dietrich, S., Tavani, M., Tiberia, A., & Porcù, F. (2019, dec). Analysis of Thunderstorms Producing Terrestrial Gamma Ray Flashes With the Meteosat Second Generation. *Journal of Geophysical Research: Atmospheres*, *124*(23), 12667–12682. Retrieved from `https://onlinelibrary.wiley.com/doi/abs/10.1029/2018JD030149` doi: 10.1029/2018JD030149

Wilson, C. T. R. (1925). The electric field of a thunderstorm and some of its effects. *Proceedings of the Royal Society of London*, *37*(32D), 32D–37D. doi: 10.1088/1478-7814/37/1/314

Xu, W., Celestin, S., & Pasko, V. P. (2012, apr). Source altitudes of terrestrial gamma-ray flashes produced by lightning leaders. *Geophysical Research Letters*, *39*(8). Retrieved from `http://doi.wiley.com/10.1029/2012GL051351` doi: 10.1029/2012GL051351

GEOPHYSICAL RESEARCH LETTERS

Supporting Information for "Spectral Observations of Optical Emissions Associated with Terrestrial Gamma-Ray Flashes"

Matthias Heumesser[1], Olivier Chanrion[1], Torsten Neubert[1], Hugh Christian[2], Christoph Köhn[1], Krystallia Dimitriadou[1], Francisco J. Gordillo-Vazquez[3], Alejandro Luque[3], Francisco Javier Prez-Invernón[3,4], Richard J. Blakeslee[5], Andrey Mezentsev[6], Nikolai Østgaard[6] and Victor Reglero[7].

[1]National Space Institute, Technical University of Denmark (DTU Space), Denmark

[2]Earth System Science Center, University of Alabama in Huntsville, Alabama, USA

[3]Instituto de Astrofísica de Andalucía (IAA - CSIC), Granada, Spain

[4]Deutsches Zentrum für Luft- und Raumfahrt (DLR), Oberpfaffenhofen, Germany

[5]NASA Marshall Space Flight Center, Huntsville, Alabama, USA

[6]Birkeland Centre for Space Science, University of Bergen, Norway

[7]Image Processing Laboratory, University of Valencia, Spain

Corresponding author: M. Heumesser, DTU SPACE, Technical University of Denmark, Elektrovej, Building 328, 2800 Kgs. Lyngby, Denmark. (heumat@space.dtu.dk)

Contents of this file

1. Tables S1 and S3

2. Figure S2 and S4

Introduction

This supporting information contains two more figures as well as tables for the main pulse and pre-activity parameters to make it easier to extract values for them. The description of how the data was colleced and processed is given in section 2, Measurements and Analysis, of the main manuscript.

Following the sequence of the main manuscript, we start with the main peak parameters in Table S1. Mean, median, standard deviation, the 25^{th} and 75^{th} percentile are given there for every attribute. Next, we present a boxplot purely for the pre-activty, giving start times, durations and intensities. The shape and structure follows Figure 3 from the main text. Table S3 gives the respective values in the same form as Table S1. Last, we include a scatter plot showing how the fit parameter τ and the FWHM in the 337 nm band correlate for the main pulses associated to TGFs. The respective fit we give in the manuscript is shown too.

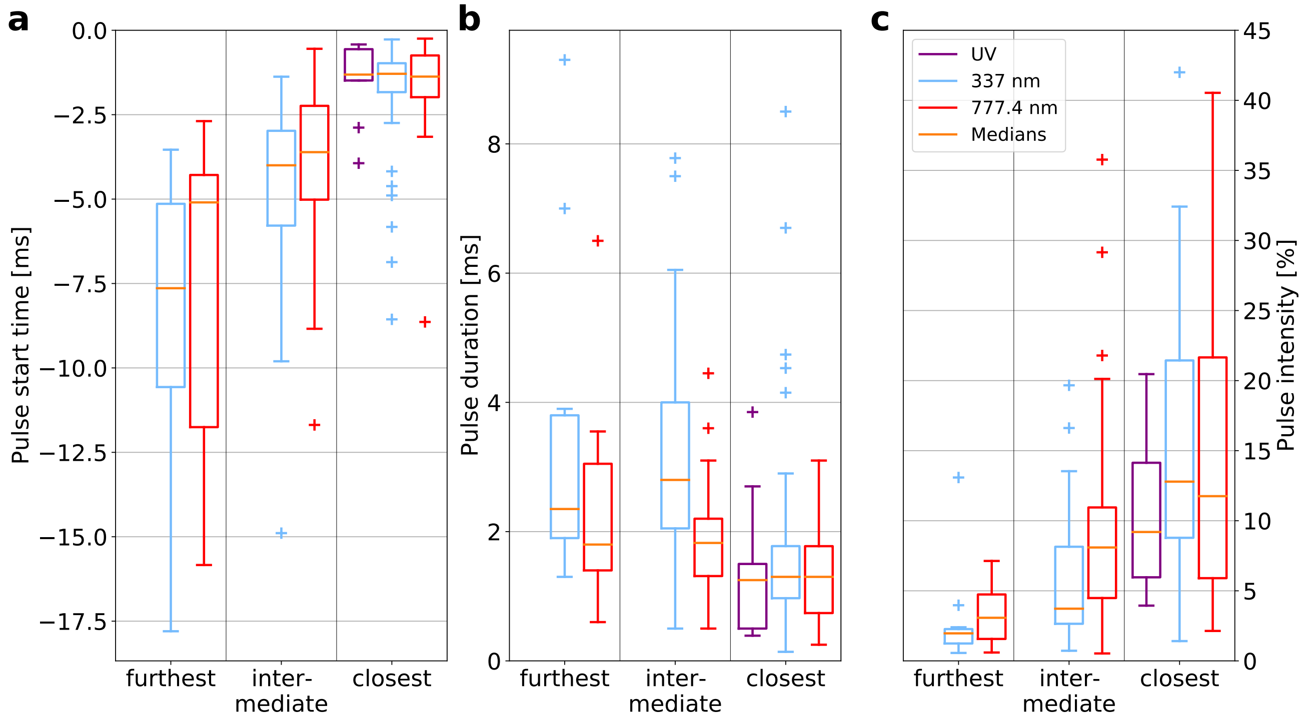

Figure S2. Characteristics of the pre-activity. The start times are relative to the start of the main optical pulse, while intensities are given in percent of the main peak maximum. The box definitions are as for Figure 3. Panel (**a**) repeats the start time, panel (**b**) shows the pulse durations and panel (**c**) the instensity development.

Table S1. Values for the main peak parameters presented in Figure 3 of the main text. All attributes are given as mean μ, standard deviation σ of the sample, 25th quartile, median and 75th quartile. The source time is relative to the first TGF photon, taken as 0 ms and was only determined in the 337 nm band.

	337 nm					777.4 nm					F/MUV				
	μ	σ	25Q	*Median*	75Q	μ	σ	25Q	*Median*	75Q	μ	σ	25Q	*Median*	75Q
Source start [ms]	0.38	1.05	-0.11	*-0.01*	0.21			-					-		
Rise time [ms]	0.39	0.17	0.29	*0.37*	0.44	0.33	0.14	0.24	*0.29*	0.39	0.29	0.10	0.23	*0.26*	0.33
FWHM [ms]	1.39	0.51	0.97	*1.26*	1.76	0.93	0.29	0.75	*0.88*	1.14	0.91	0.25	0.64	*0.90*	1.13
Peak value [μW/m^2]	60.03	36.87	24.77	*58.51*	77.67	21.76	19.17	7.08	*17.27*	32.47	60.54[a]	29.08[a]	39.09[a]	*55.59*[a]	70.50[a]
Linear ratio 337/777 [1]	3.77	1.85	2.52	*3.18*	4.12			-					-		
Log10 ratio 337/777 [1]	0.58	0.19	0.40	*0.50*	0.61			-					-		

[a]F/MUV values have to be multiplied by 10^{-3}

Table S3. Values for the optical pre-activity before the main peak presented in Figure S2. All attributes are given as mean μ, standard deviation σ of the sample, 25^{th} quartile, median and 75^{th} quartile. The pulses are sorted relative to the start of the main peak in reverse chronological order. The intensity values for the pulses are relative to the associated main peak maximum, independently calculated before the summary statistics of the whole sample are determined.

		337 nm					777.4 nm					F/MUV				
		μ	σ	25Q	*Median*	75Q	μ	σ	25Q	*Median*	75Q	μ	σ	25Q	*Median*	75Q
closest	start [ms]	-1.79	1.65	-1.83	*-1.29*	-0.98	-1.62	1.31	-1.98	*-1.37*	-0.75	-1.49	1.12	-1.49	*-1.31*	-0.56
pulse	duration[ms]	1.71	1.54	0.97	*1.30*	1.78	1.37	0.74	0.74	*1.30*	1.78	1.44	1.09	0.50	*1.25*	1.50
	intensity [%]	15.47	10.76	8.78	*12.79*	21.44	17.17	15.95	5.90	*11.75*	21.65	39.98	85.62	5.96	*9.20*	14.14
intermediate	start [ms]	-5.00	3.06	-5.79	*-4.00*	-2.98	-4.13	2.50	-5.02	*-3.61*	-2.24			-		
pulse	duration [ms]	3.34	1.82	2.05	*2.80*	4.00	1.87	0.96	1.31	*1.82*	2.20			-		
	intensity [%]	6.05	4.97	2.65	*3.72*	8.14	10.12	8.55	4.48	*8.09*	10.95			-		
furthest	start [ms]	-8.63	4.56	-10.57	*-7.64*	-5.14	-7.79	4.61	-11.75	*-5.10*	-4.29			-		
pulse	duration [ms]	3.34	2.24	1.90	*2.35*	3.80	2.39	1.61	1.40	*1.80*	3.05			-		
	intensity [%]	2.63	3.14	1.24	*1.96*	2.27	7.68	14.79	1.57	*3.07*	4.74			-		

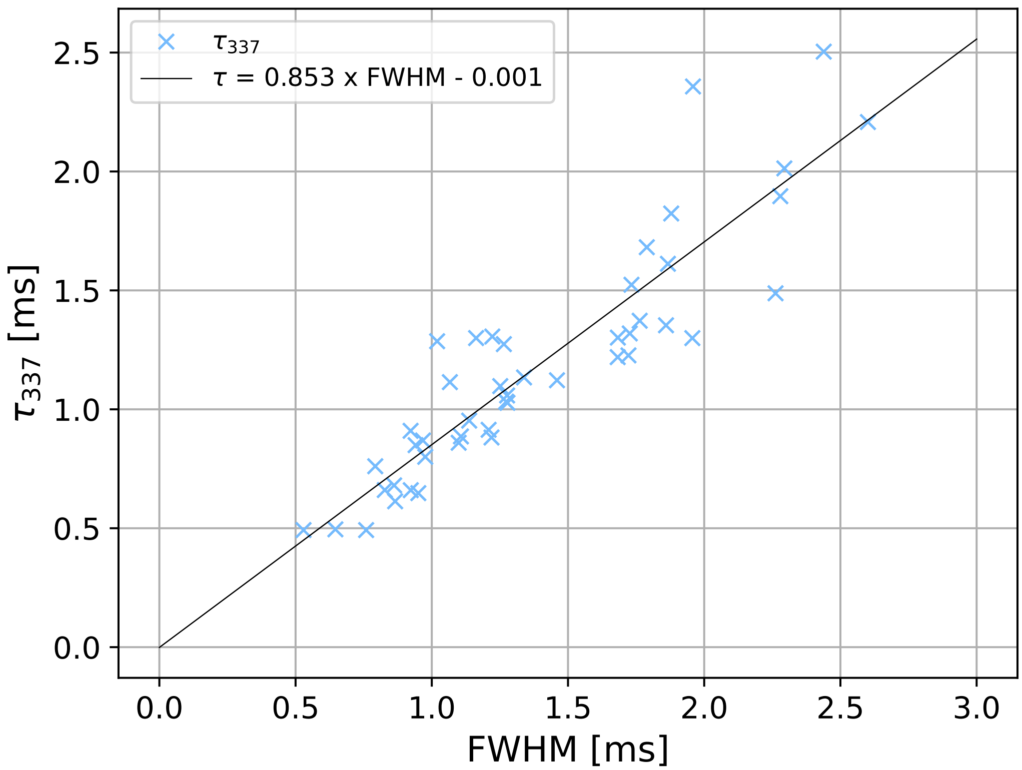

Figure S4. Fit parameter τ compared to the FWHM, both in the 337 nm band. The plot shows the data points for τ and the FWHM as well as the linear fit quantifying their correlation we give in the manuscript. Its equation is repeated in the legend of the plot.